metals

MDPI

Article

The Effect of Mn on the Mechanical Properties and In Vitro Behavior of Biodegradable Zn-2%Fe Alloy

Lital Ben Tzion-Mottye, Tomer Ron *, Dan Eliezer and Eli Aghion

Department of Materials Engineering, Ben-Gurion University of the Negev, Beer-Sheva 8410501, Israel; bentzlit@post.bgu.ac.il (L.B.T.-M.); deliezer@bgu.ac.il (D.E.); egyon@bgu.ac.il (E.A.)
* Correspondence: toron@post.bgu.ac.il

Abstract: The attractiveness of Zn-based alloys as structural materials for biodegradable implants mainly relates to their excellent biocompatibility, critical physiological roles in the human body and excellent antibacterial properties. Furthermore, in in vivo conditions, they do not tend to produce hydrogen gas (as occurs in the case of Mg-based alloys) or voluminous oxide (as occurs in Fe-based alloys). However, the main disadvantages of Zn-based alloys are their reduced mechanical properties and their tendency to provoke undesirable fibrous encapsulation due to their relatively high standard reduction potential. The issue of fibrous encapsulation was previously addressed by the authors via the development of the Zn-2%Fe alloy that was selected as the base alloy for this study. This development assumed that the addition of Fe to pure Zn can create a microgalvanic effect between the Delta phase ($Zn_{11}Fe$) and the Zn-matrix that significantly increases the biodegradation rate of the alloy. The aim of the present study is to examine the effect of up to 0.8% Mn on the mechanical properties of biodegradable Zn-2%Fe alloy and to evaluate the corrosion behavior and cytotoxicity performance in in vitro conditions. The selection of Mn as an alloying element is related to its vital role in the synthesis of proteins and the activation of enzyme systems, as well as the fact that Mn is not considered to be a toxic element. Microstructure characterization was carried out by optical microscopy and scanning electron microscopy (SEM), while phase analysis was obtained by X-ray diffraction (XRD). Mechanical properties were examined in terms of hardness and tensile strength, while corrosion performance and electrochemical behavior were assessed by immersion tests, open circuit potential examination, potentiodynamic polarization analysis and impedance spectroscopy. All the in vitro corrosion testing was performed in a simulated physiological environment in the form of a phosphate-buffered saline (PBS) solution. The cytotoxicity performance was evaluated by indirect cell viability analysis, carried out according to the ISO 10993-5/12 standard using Mus musculus 4T1 cells. The obtained results clearly demonstrate the strengthening effect of the biodegradable Zn-2%Fe alloy due to Mn addition. The effect of Mn on in vitro corrosion degradation was insignificant, while in parallel Mn had a favorable effect on indirect cell viability.

Keywords: biodegradable implants; cell viability; in vitro; zinc; Zn–Fe–Mn

Citation: Ben Tzion-Mottye, L.; Ron, T.; Eliezer, D.; Aghion, E. The Effect of Mn on the Mechanical Properties and In Vitro Behavior of Biodegradable Zn-2%Fe Alloy. *Metals* **2022**, *12*, 1291. https://doi.org/10.3390/met12081291

Academic Editor: Dalibor Vojtech

Received: 6 July 2022
Accepted: 28 July 2022
Published: 30 July 2022

1. Introduction

Biodegradable metallic materials are being extensively investigated, mainly due to their improved mechanical properties compared with their counterpart polymeric-based systems [1,2]. In addition, biodegradable metals tend to present adequate combination of degradability and biocompatibility characteristics, and hence are considered to be potential structural materials for various applications, such as orthopedic implants and cardiovascular devices [3–5]. The manufacturing process of biodegradable alloys mainly include casting, plastic forming, powder metallurgy and lately advanced additive manufacturing technology [6–9]. Biodegradable metals basically aim at replacing permanent biomaterial implants such as titanium alloys, stainless steel, cobalt–chromium alloys and others in applications where eventually the implants are not necessary after full recovery is reached [10,11].

Furthermore, permanent implants may cause discomfort, premature failure (mainly due to stress corrosion) and, in rare cases, a chronic inflammatory response that requires a second operation to remove the implant [3,6,12,13]. The development of innovative biodegradable metal implants is mainly focused on using Fe-, Mg- and Zn-based alloys due to their acceptable biocompatibility performance. However, Fe-based alloys tend to generate insufficient degradation rates and, consequently, produce voluminous oxide that can encourage inflammation and repulse neighboring biological matrices [4,14–21]. As for Mg-based alloys, these mainly suffer from accelerated corrosion degradation [22] that is accompanied by hydrogen gas evolution, which can lead to the danger of gas embolism [7,23–34]. In contrast to Fe- and Mg-based alloys, Zn alloys do not tend to generate either voluminous oxide or hydrogen gas in in vivo conditions [27,35–37]. In addition, Zn plays several crucial physiological roles in the human body, such as being a functional element in more than 300 enzymes and its involvement in nucleic acid metabolism. It is also believed to act as an antibacterial and antiviral constituent [27,38–41]. Nevertheless, the disadvantage of pure zinc is the danger of relatively high levels of anemia, unsatisfactory mechanical properties and the risk of fibrous encapsulation due to its relatively high potential (−0.762 V) [2,21]. The alloy-based matrix (Zn-2%Fe) selected for this study has already been developed and studied by the authors of this paper [21,30] and was found to be a possible solution to overcome the danger of fibrous encapsulation. Apparently, the addition of Fe to pure Zn created a microgalvanic effect between the Delta phase ($Zn_{11}Fe$) and the Zn-matrix, which consequently doubled the degradation rate of the alloy in both in vitro and in vivo conditions [21,30]. The aim of this study is to evaluate the effect of up to 0.8%Mn on the mechanical properties of Zn-2%Fe alloy, as well as to examine the corrosion degradation and cytotoxicity performance of this material system in in vitro conditions. The proposed addition of Mn to biodegradable Zn-2%Fe alloy is supported by the fact that Mn is not considered to be a toxic element [5], and its recommended intake is about 2 mg per day [42]. In addition, Mn plays a vital role in the synthesis of proteins and the activation of enzyme systems [6]. Deficiency of Mn in the human body may provoke diseases such as diabetes, osteoporosis and atherosclerosis [6,39,43]. The selection of up to 0.8% Mn additions was due to the assumption that the maximum solubility of Mn in Zinc is 0.8% [44] and based on the fact that Mn can improve castability, and hence the properties, of Zn-base alloys [5].

2. Experimental Procedure

2.1. Alloy Preparation

The Zn-2%Fe-based alloys with different amounts of Mn (0.3%, 0.6% and 0.8%) were produced by gravity casting. This was carried out using a graphite crucible and highly purified raw materials in the form of Zn bars, Fe powder and Mn powder, having average particle sizes of 42 and 50 μm, respectively. The melting temperature was 700 °C and melt was mixed for 2 h, while stirring took place every 30 min. The molten alloy was casted in the form of rods within a steel die having the dimensions of: 16 cm length and 6 cm diameter.

To upgrade the properties of the casted alloy, a subsequent extrusion process was performed. This was due to the assumption that a hot-working process along with annealing can significantly improve the mechanical properties [44]. Accordingly, the as-cast rods were turned into 13 mm diameter billets and exposed to a homogenization treatment of 2 h at 200 °C that was followed by an extrusion process to obtain rods with a final diameter of 6 mm. The chemical composition of the tested alloys was analyzed using an Inductively Coupled Plasma Optical Emission Spectrometer (ICP-SPECTRO, ARCOS FHS-12, Kelve, Germany) and the obtained results are summarized in Table 1.

Table 1. The chemical composition of the tested alloys (wt.%).

Tested Alloy	Fe	Mn	Cu	Ca	Zn
Zn-2%Fe	1.9	0.005	0.006	0.007	Balance
Zn-2%Fe-0.3%Mn	1.7	0.3	0.004	0.01	Balance
Zn-2%F-0.6%Mn	1.7	0.6	0.007	0.007	Balance
Zn-2%Fe-0.8%Mn	1.8	0.8	0.003	0.004	Balance

2.2. Microstructure Characterization

The microstructure of the tested alloys was evaluated after polishing and etching in 5% Nital solution that was composed of 5 mL HNO_3 and 100 mL ethanol. The microscopic characterization was performed using a scanning electron microscopy (SEM), JEOL JSM-5600 (JEOL, Tokyo, Japan) combined with energy-dispersive X-ray spectroscopy (EDS, -Thermo Fisher Scientific, Waltham, MA, USA) for spot chemical analysis. The identification of phases was carried out using X-ray diffraction (XRD) analysis (RIGAKU-2100H, Tokyo, Japan) with Cu-Kα at 40 kV and 30 mA, and the scanning rate was 0.02°/min.

2.3. Mechanical Property Examinations

The mechanical properties of the tested alloys were examined in terms of hardness and tensile strength. The hardness examination was performed by Vickers measurements (Zwick/Roell Indentec, Quantarad Technologies, Selangor, Malaysia) with an applied load of 5 kg (HV5). Tensile testing was performed using a CORMET facility (C76, Cormet Testing Systems, Vantaa, Finland) at a constant strain rate of 0.5 mm/min using 3 specimens of each alloy.

2.4. Corrosion Performance and Electrochemical Behavior

The corrosion performance of the alloys in immersion tests was evaluated in a simulated physiological environment in the form of PBS solution at 37 °C, for 14 days. The corrosion rate was evaluated by calculating the weight loss according to the ASTM G2 standard using 3 samples from each group. The corrosion products at the external surface were examined by SEM analysis and later removed using an ultrasonic bath and ethanol for corrosion rate measurements.

Assessment of the electrochemical behavior was carried out in the form of open circuit potential (OCP) measurements, potentiodynamic polarization analysis and impedance spectroscopy. The tests were performed using a Bio-Logic SP-200 potentiostat (BioLogic Science Instruments, Seyssinet-Pariset, France), quipped with EC-Lab software V11.18. The electrochemical cell was in the form of a three-electrode cell using saturated calomel (SCE) as a reference electrode, a platinum electrode as an auxiliary electrode and the tested alloy as the working electrode [45]. All the electrochemical test analyses were carried out in a PBS solution at room temperature and performed 3 times. The exposure time of the open circuit potential measurements was nearly 90 h—until a steady potential was obtained. The scanning rate used by the potentiodynamic polarization analysis was 1 mV/s and Tafel extrapolation was used to determine the corrosion rate. The impedance spectroscopy measurements were carried out between 10 kHz and 100 mHz using a 10 mV amplitude above the open circuit potential.

2.5. Cytotoxicity Analysis

The cytotoxicity analysis of the tested alloys was carried out by assessing the effect of indirect extract cell metabolic activity, in accordance with the ISO 10993-5/12 standard. The selected cells were Mus musculus 4T1 cells due to their relatively increased sensitivity to toxic effects. Four cylindrical samples with the dimensions of D = 10 mm and h = 2 mm were prepared from each of the tested alloys. For reference, Ti-6Al-4V alloy was selected for comparison. All the tested samples were initially polished to 4000 grits and ultrasonically cleaned for 10 min with ethanol and 5 min with acetone. After air drying, the samples

were sterilized in UV light for 1 h on each side. The tested Zn-base alloys and the reference Ti-6Al-4V alloy were incubated for 24 h in Dulbecco Modified Eagle's Medium (DMEM) supplemented with 4.5 g L^{-1} D-Glucose, 10% Fetal Bovine Serum (FBS), 4 mM L-Glutamine, 1 mM Sodium Pyruvate and 1% Penicillin Streptomycin Neomycin (PSN) antibiotic mixture at 37 °C in a humidified atmosphere. The surface area-to-volume ratio was 1.25 cm^2 per 1mL. The 4T1 cells were seeded in two 96-well plates, with a concentration of 5000 cells per well for 24 h to allow cell attachment to the surface. Subsequently, the liquid from the cell plates was replaced by 100 µL of filtered alloy extracts, with concentrations of 10%; in order to adequately simulate in vivo conditions, the filtration was carried out using a PVDF membrane (0.45 µm) [46,47]. The positive control group containing cell wells with only DMEM aims to represent the opposite control groups that contain cells with 90% DMEM and 10% DMSO. This process was carried out on two identical 96-well plates that where incubated for 24 h and 48 h. The assessment of cell viability was obtained after 24 h and 48 h of incubation using a Cell Proliferation kit (XTT, Biological Industry, Beit Haemek, Israel). The process included collecting all the liquid from the cell wells and replacing it with the mixture of 50 µL reagent and 1 µL activator to 100 µL DMEM for each well, while using an incubation period of 2 h. The liquid color was measured spectrophotometrically at 490 nm using a microplate reader (SYNERGY-Mx, BioTek, Winooski, VT, USA). Assessment of cell viability was consequently calculated and compared with the control blank wells.

3. Results

Phase identification by XRD analysis of Zn-2%Fe alloys with up to 0.8% Mn revealed the presence of three dominating phases: Pure Zn, Fe-rich phase and Mn-rich phase as shown in Figure 1. The Fe-rich phase was identified as $Zn_{11}Fe$, and the Mn-rich phase was classified as $(Fe,Mn)Zn_{13}$ [39,48].

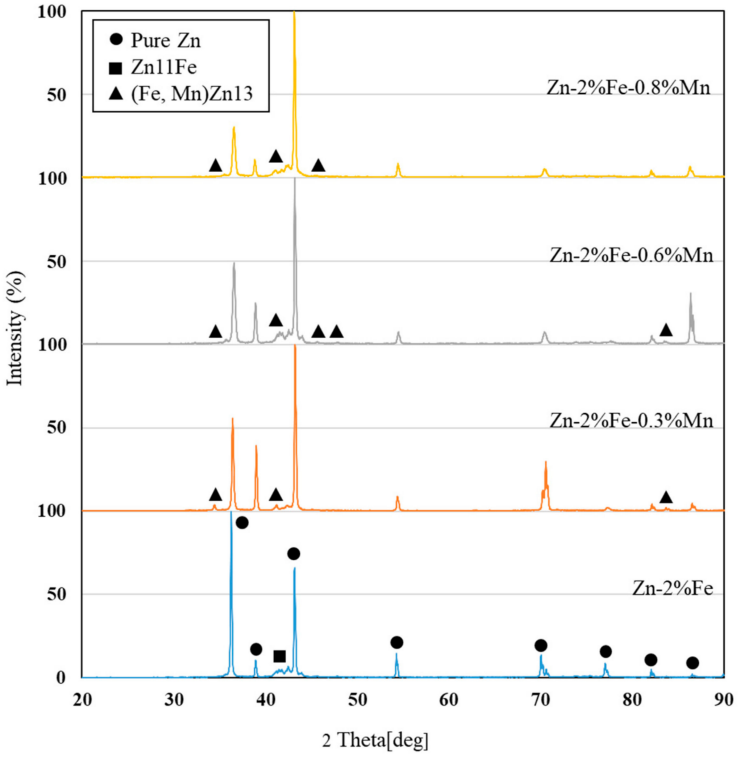

Figure 1. X-ray analysis of Zn-2%Fe alloys with up to 0.8%Mn.

Typical microstructure, as derived by optical microscopy of Zn-2%Fe alloys with up to 0.8% Mn post extrusion process, is shown in Figure 2. This reveals a finer homogenized microstructure with some degree of preferred orientation post extrusion, as expected. SEM examination of the alloy with the highest content of Mn (0.8%) post extrusion is shown

in Figures 3 and 4, along with spot chemical composition analysis of the main phases, as shown in Table 2. The three dominant phases were identified as Zn-base matrix, $Zn_{11}Fe$ and (Fe, Mn)Zn_{13}, which clearly comes in line with the results obtained by the XRD analysis. The Zn-base matrix included some amount of Fe (0.4%) and Mn (0.9%), which indicates that those alloying elements were also partly dissolved in Zinc. In terms of structural appearance, while the main precipitate $Zn_{11}Fe$ appears as a blocky phase, the secondary phase (Fe, Mn)Zn_{13} was relatively finer and well-spread within the Zn-base matrix.

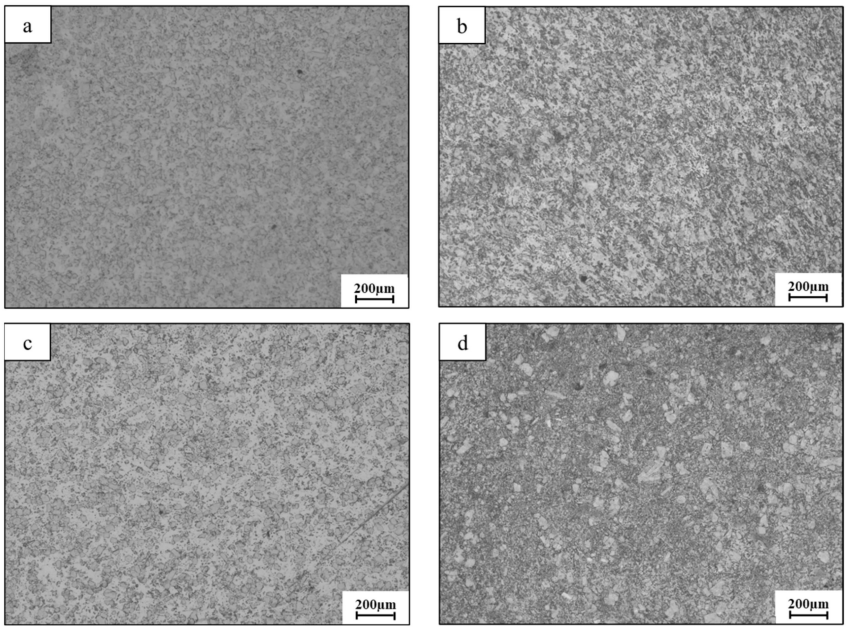

Figure 2. Optical microscopy in post extrusion process condition of Zn-2%Fe with up to 0.8% Mn: (**a**) Zn-2%Fe; (**b**) Zn-2%Fe-0.3%Mn; (**c**) Zn-2%Fe-0.6%Mn; (**d**) Zn-2%Fe-0.8%Mn.

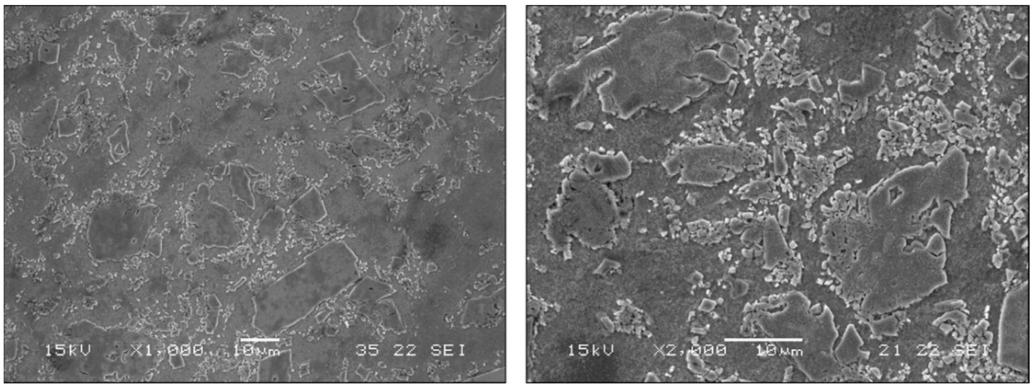

Figure 3. General view obtained by SEM of Zn-2%Fe-0.8%Mn alloy.

Table 2. Spot chemical composition by SEM-EDS analysis (wt.%) of different areas shown in Figure 5.

Point	Zn	Fe	Mn	Dominant Phases
1	98.7 ± 0.3	0.4 ± 0.2	0.9 ± 0.1	Zn base matrix
2	91.3 ± 1	7.5 ± 0.8	1.2 ± 0.2	$Zn_{11}Fe$
3	96.3 ± 0.9	2.2 ± 0.7	1.5 ± 0.3	(Fe, Mn)Zn_{13}

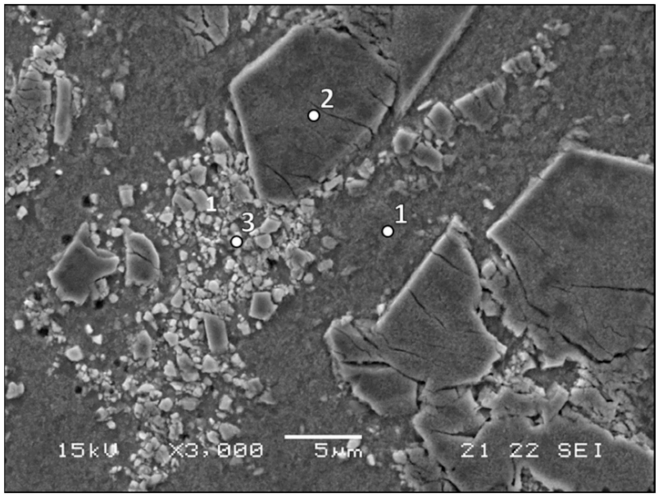

Figure 4. Close-up view by SEM of Zn-2%Fe-0.8%Mn alloy.

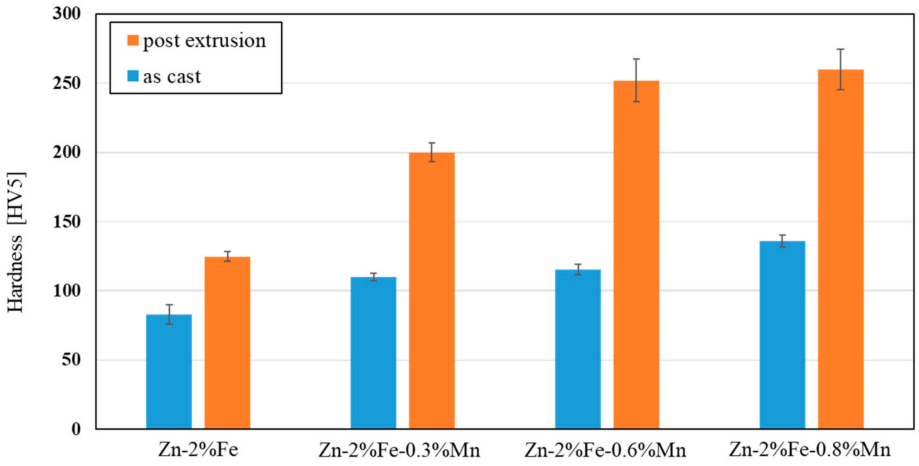

Figure 5. Hadrness measurement of Zn-2%Fe alloy with Mn additions in as-cast and post extrusion conditions.

Figure 4 and Table 2 present the EDS analysis that was conducted for three main areas: Zn base matrix, $Zn_{11}Fe$ and (Fe, Mn)Zn_{13}.

The effect of Mn on the mechanical properties of a Zn-2%Fe alloy in terms of hardness and tensile strength is presented in Figures 5 and 6, respectively, along with the actual values of yield point (Y.P.), ultimate tensile strength (UTS) and elongation (post extrusion) in Table 3. This clearly shows that the hardness of all the tested alloys was significantly enhanced by the extrusion process, while an additional increase in hardness was generated as the Mn content went from 0.3% to 0.8%. In parallel, the increased amount of Mn generated higher measurements of tensile strength in terms of Y.P. (from 75 MPa to 200 MPa) and UTS (from 125 MPa to 233 MPa), while reducing ductility (from 13% elongation to 8.1%).

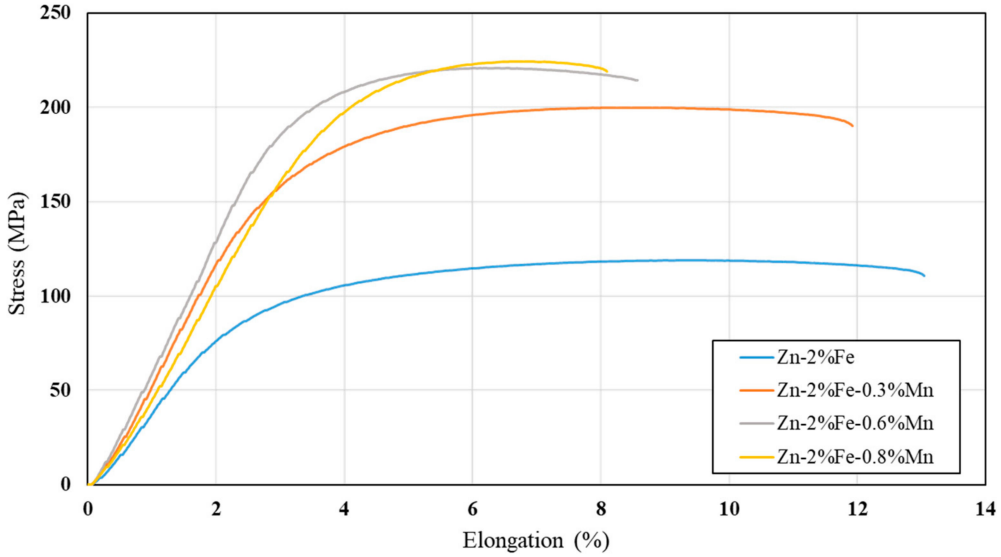

Figure 6. Tyical tensile test analysis results of the tested alloys.

Table 3. Mechanical properties derived from tensile tests shown in Figure 7.

Tested Alloy	Y.P (MPa)	UTS (MPa)	Elongation (%)
Zn-2%Fe	69 ± 4	119 ± 9	13 ± 1
Zn-2%Fe-0.3%Mn	136 ± 8	199 ± 12	12 ± 2
Zn-2%Fe-0.6%Mn	177 ± 10	221 ± 13	8.5 ± 1
Zn-2%Fe-0.8%Mn	191 ± 7	224 ± 9	8.1 ± 2

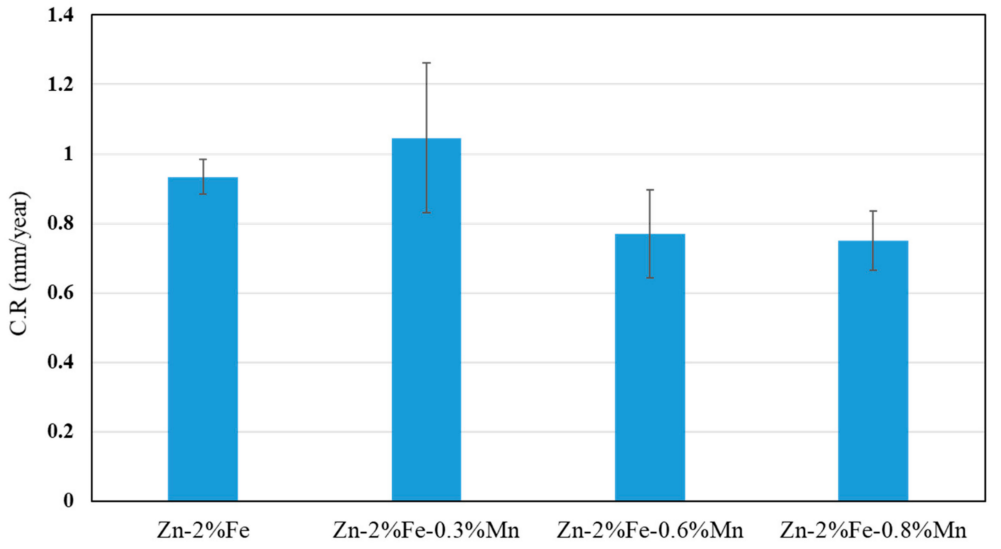

Figure 7. Corrosion rate measurements of Zn-2%Fe with up to 0.8% Mn after immersion test in PBS solution for 14 days.

The corrosion rate measurements of the tested alloys in a simulated physiological environment, as calculated from the immersion tests in PBS solution at 37 °C for 14 days, is presented in Figure 7. This reveals that the addition of up to 0.8%Mn has a minor effect on the corrosion rate of the reference-based alloy Zn-2%Fe. Close-up examination of the corrosion products at the surface of the tested alloy highlights the microgalvanic corrosion mechanism that took place, as shown in Figure 8. Apparently, the main precipitate phase $Zn_{11}Fe$ with a blocky appearance and relatively sharp edges was nearly unattacked, while the surrounding Zn-base matrix was heavily corroded. This was mainly due to the

differences in the corrosion potential between the two phases. The corrosion potential of $Zn_{11}Fe$ is −0.87 $V_{SCE,}$ while that of the matrix that surrounds this precipitate is −1.03 V_{SCE}. This consequently created a microgalvanic corrosion process where the $Zn_{11}Fe$ precipitate is more cathodic than the Zn-base matrix [21,49].

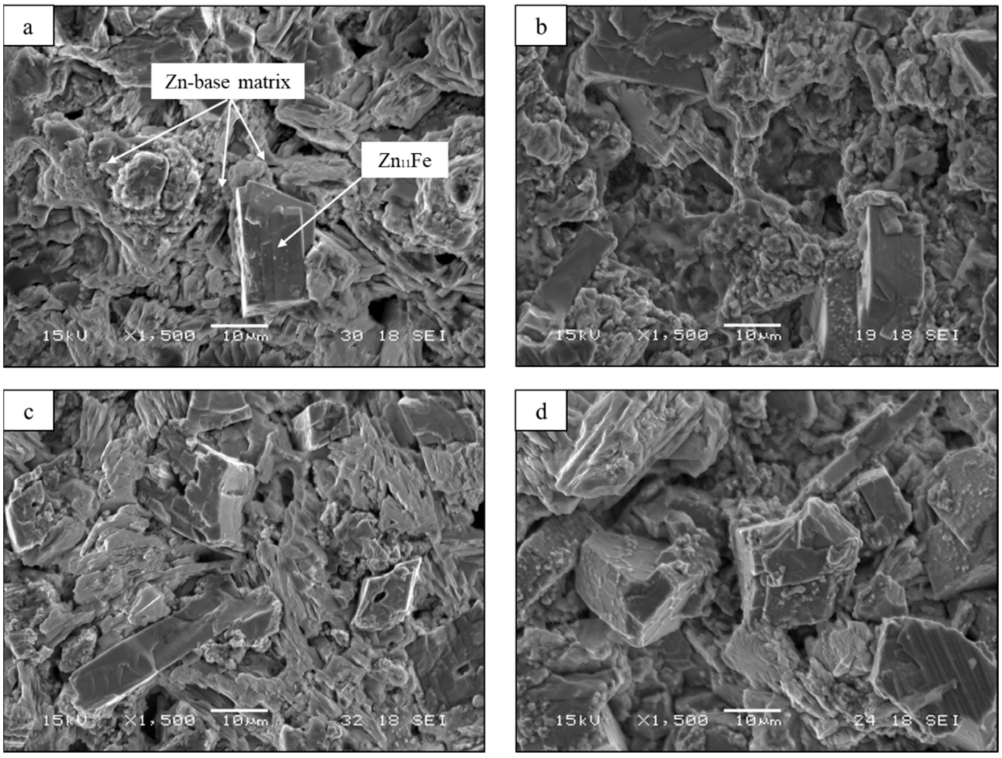

Figure 8. Close-up views of the corrosion products at the external surface of tested alloys after immersion test in PBS solution for 14 days. (**a**–**d**) Same specimen in different location.

Measurements of the open circuit potential (OCP) of the tested alloys, immersed in PBS solution for up to 90 h, is presented in Figure 9. The OCP of all tested alloys was within the range of −1.04 V and −1.09 V, with an arbitrary effect of Mn addition. This, in practice, means that the effect of Mn on OCP was insignificant, as indicated by the immersion tests.

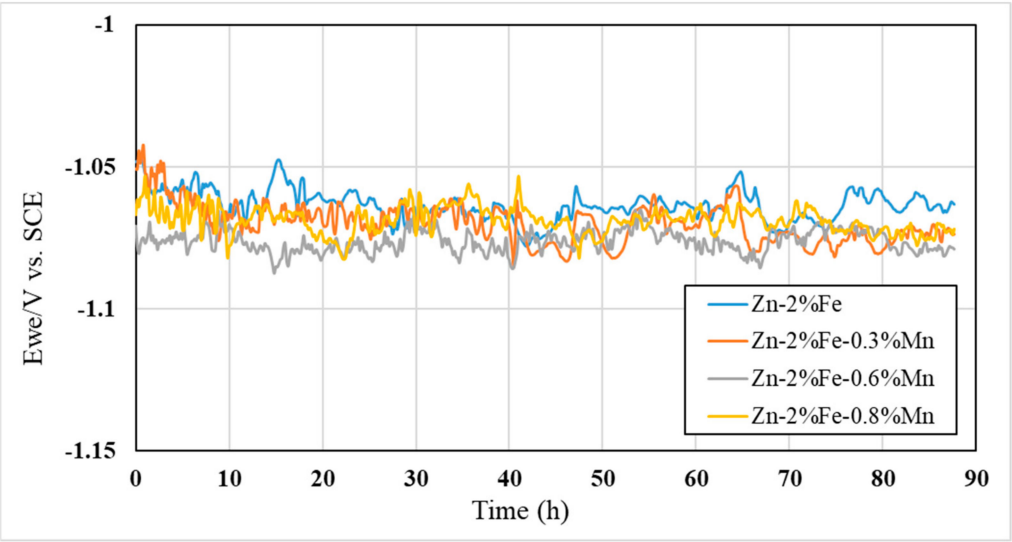

Figure 9. Open circuit potential of tested alloys in PBS solution.

Potentiodynamic polarization analyses are shown in Figure 10 and Table 4. These reveal that the nature of the polarization curves due to the additions of Mn to the base alloy is quite uniform. Furthermore, the corrosion potential and corrosion rate measurements of the tested alloys in terms of Tafel extrapolation were also relatively similar. The results of the potentiodynamic polarization analysis basically come in line with the impedance spectroscopy (EIS) evaluation in terms of the Nyquist diagram, as shown in Figure 11. According to this evaluation, the magnitude of the radii of curvature of the tested alloys was quite similar. As the radii of curvature essentially represent the surface corrosion resistance, it is again evident that the effect of Mn on the corrosion resistance of the base Zn-2%Fe alloy was relatively minor.

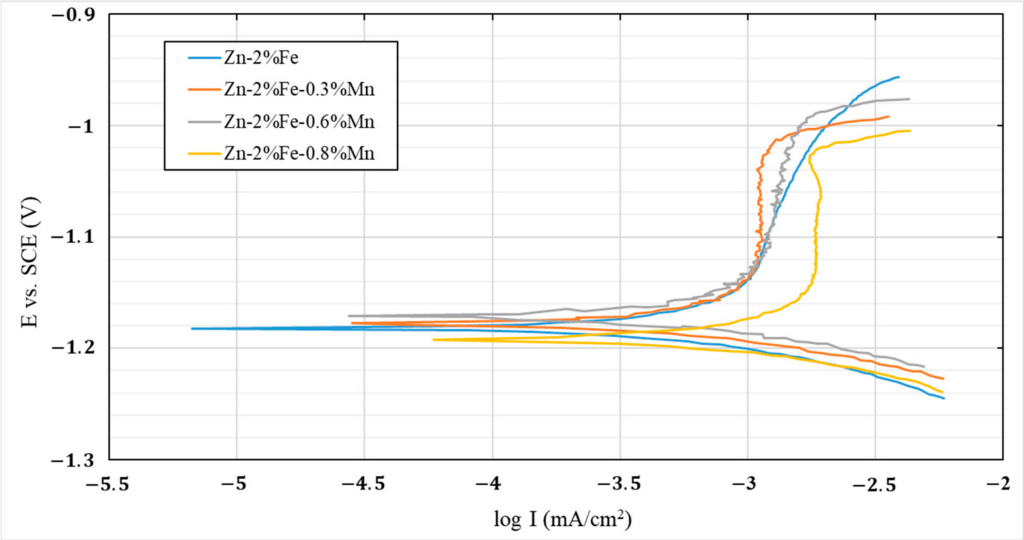

Figure 10. Potentiodynamic polarization curves of tested alloys as obtained in PBS solution.

Table 4. Electrochemical parameters and corrosion rates by Tafel extrapolation generated from the potentiodynamic polarization analysis shown in Figure 10.

Corrosion Parameter	Zn-2%Fe	Zn-2%Fe-0.3%Mn	Zn-2%Fe-0.6%Mn	Zn-2%Fe-0.8%Mn
Ecorr (V)	−1.182 ± 0.09	1.177 ± 0.02	−1.171 ± 0.01	−1.192 ± 0.01
I- corrosion current density (μA/cm^2)	1.353 ± 0.1	1.478 ± 0.3	1.61 ± 0.2	2.314 ± 0.3
C.R (mmpy)	0.072 ± 0.006	0.079 ± 0.01	0.086 ± 0.001	0.124± 0.02

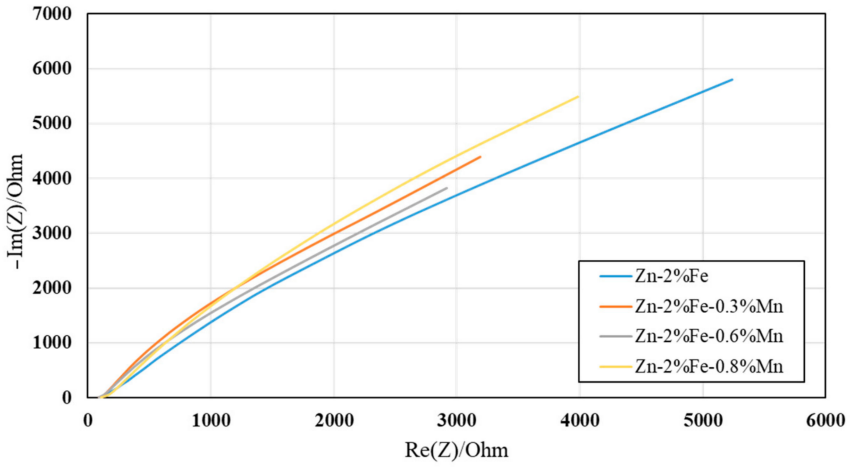

Figure 11. Impedance spectroscopy analysis of the tested alloys in PBS solution in terms of Nyquist diagram.

Cytotoxicity examination of the tested alloys carried out by indirect cell viability analysis using Ti-6%Al-4%V as a reference alloy, and incubation periods of 24 h and 48 h are shown in Figure 12. This reveals that the cell viability of all the tested alloys was clearly above 95% and 120% after 24 and 48 h of incubation, respectively. In fact, this result comes in line with the requirements mentioned by ISO 10993-5 [50], which indicate that adequate cell viability should be above 70% to prevent negative cytotoxic effects. As for the influence of Mn additions to the base Zn-2%Fe alloy, the addition of up to 0.8% Mn has some relative beneficial effect on cell viability, especially for the longer incubation time. The above quantitative results are also supported by the general appearance and healthy conditions of the 4T1 cells after 48 h incubation, as shown in Figure 13.

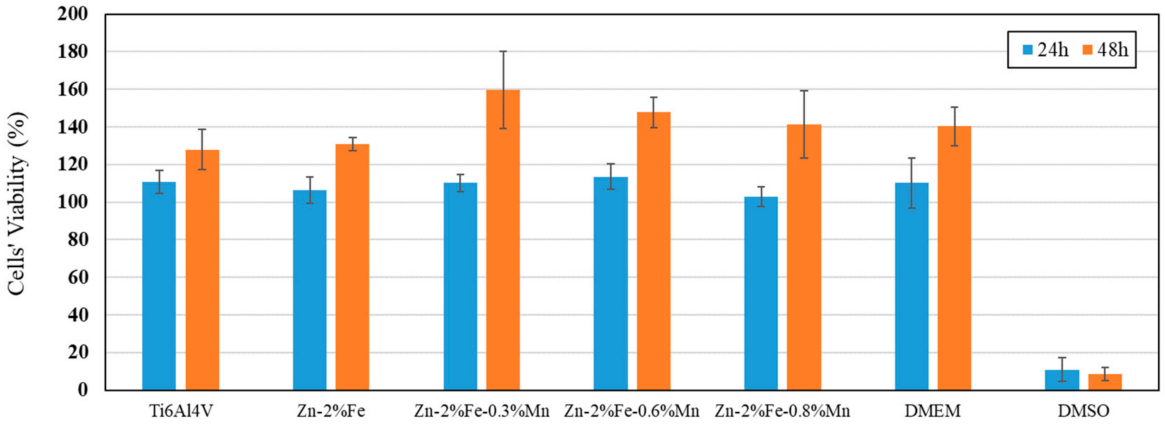

Figure 12. Indirect cell viability analysis of the tested alloy after incubation times of 24 and 48 h.

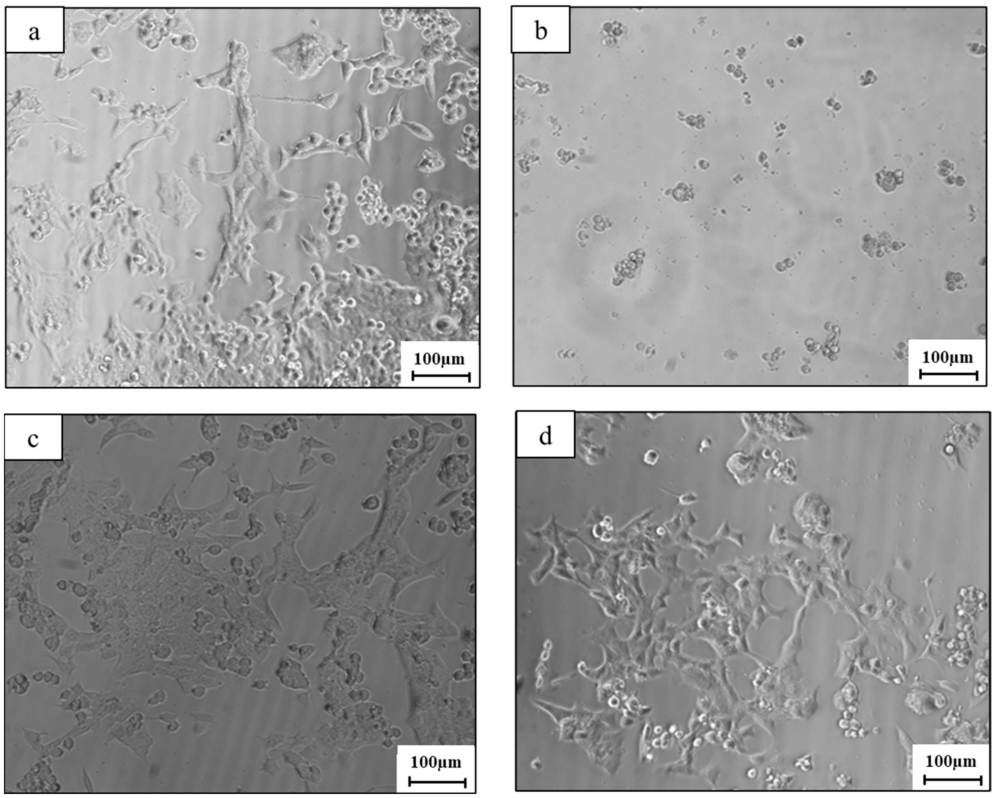

Figure 13. *Cont.*

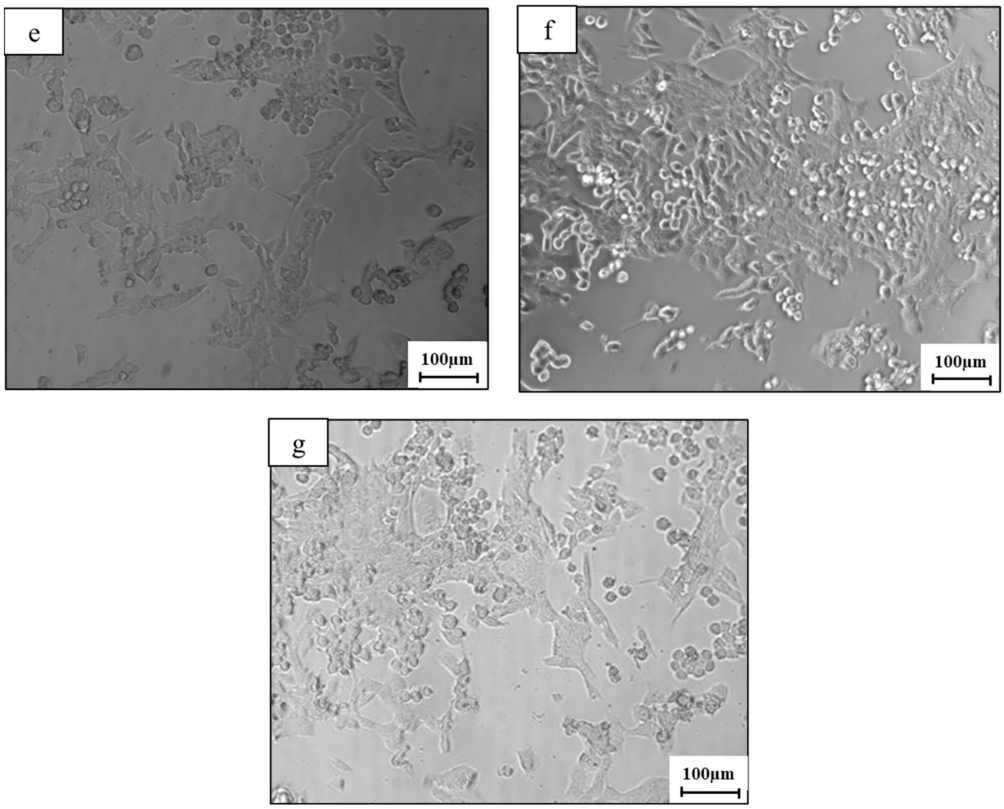

Figure 13. General view of 4T1 cells after 48h of incubation: (**a**) DMEM only; (**b**) DMEM+DMSO; (**c**) TI6Al4V; (**d**) Zn-2%Fe; (**e**) Zn-2%Fe-0.3%Mn; (**f**) Zn-2%Fe-0.6%Mn; (**g**) Zn-2%Fe-0.8%Mn.

4. Discussion

The strengthening effect of biodegradable Zn-2%Fe alloy due to additions of up to 0.8%Mn was demonstrated in terms of a significant increase in the yield point and ultimate tensile strength. As the solubility of Mn in Zn-based alloys is limited to a about 0.8%Mn [44], it is believed that the main mechanism of strength enhancement is obtained by solution strengthening [5]. Nevertheless, some additional hardening could also be generated due to the production of a minor amount of the precipitation phase (Fe, Mn)Zn_{13}. According to Zhi Shi et al. [39], this phase is generated due to the capability of Mn to replace about 18–71% of Fe in the $FeZn_{13}$ phase. Furthermore, they claimed that (Fe, Mn)Zn_{13} can have a core/shell structure of (Fe, Mn)Zn_{13}/$MnZn_{13}$, respectively, with a coherent orientation relationship that enhances brittleness. The slight reduction in the ductility of biodegradable Zn-2%Fe alloy (from 13% elongation to just above 8%) due to the addition of 0.8% Mn is tolerable, as it still maintains the adequate engineering ductility that is required from biodegradable implant materials [51].

Despite the favorable effect of Mn on strength, it was evident that the addition of up to 0.8% Mn did not have any significant effect on the corrosion performance of the Zn-2%Fe alloy in a simulated physiological environment, as shown in Figure 7. It is believed that this may be related to the balanced effect of Mn on the in vitro corrosion degradation mechanism. On one hand, Mn tends to react with heavy metal elements such as Fe during casting, which reduces their deteriorating effect on corrosion resistance and consequently reduces the corrosion degradation process [52,53]. However, on the other hand, the differences between the standard potential of the Zn-based matrix (−0.762 V) and that of Mn (−1.18 V) [54] increase the possibility of creating microgalvanic cells that can increase the corrosion degradation [5].

Regarding the cytotoxicity assessment of biodegradable Zn-2%Fe alloy with up to 0.8% Mn by indirect cell viability analysis, the obtained results indicate a favorable effect of Mn on cell viability, especially for the longer incubation time (48 h). This was manifested

by quantitative analysis (cell viability above 70% according to ISO 10993-5) [50] and by the general healthy appearance of the 4T1 cells post incubation. In fact, these results come in line with the study of Prasadh et al. [55] regarding the cell viability analysis of Mg-2%Zn-1%Ca with additions of Mn. They found that the additions of up to 0.5%Mn enhanced cell viability, mainly by increasing the cell differentiation rate. Comparable results were also found by Wang et al. in relation to Mn-doped Mg-Zn-Ca alloy [56,57].

Altogether, the main beneficial effect of adding up to 0.8% Mn to biodegradable Zn-2%Fe alloy is the favorable strengthening effect. This was obtained without damaging the biodegradability of the alloy or its cytotoxicity performance. Additional research efforts should be devoted to analyzing this innovative material system in in vivo conditions.

5. Conclusions

1. Additions of up to 0.8% Mn to biodegradable Zn-2%Fe alloy resulted in increased hardness and tensile strength in terms of yield point and ultimate tensile strength, while slightly reducing ductility. The main mechanism of strength enhancement was solution strengthening that was amplified by the precipitation hardening of a secondary phase (Fe, Mn)Zn_{13}.
2. The effect of Mn additions on the corrosion degradation of Zn-2%Fe alloy in a simulated physiological environment was insignificant. This was related to the balanced effect between reduced degradability due to Mn reaction with Fe and increased degradability attributed to the inherent microgalvanic corrosion between the Zn-based matrix and the Mn-base substance.
3. Indirect cell viability assessment showed that the addition of Mn tends to increase cell viability in in vitro conditions. This may indicate that the cytotoxicity of the Zn-2%Fe-based alloy was comparatively reduced after the addition of Mn to this alloy.

Author Contributions: L.B.T.-M.: investigation, formal analysis and writing—original draft; T.R.: investigation; D.E.: investigation; E.A.: conceptualization, methodology, supervision and writing—original draft. All authors have read and agreed to the published version of the manuscript.

Funding: This research received no external funding.

Data Availability Statement: Experimental data from this study are available from the corresponding author upon reasonable request.

Conflicts of Interest: The authors declare no conflict of interest.

References

1. Zheng, Y.F.; Gu, X.N.; Witte, F. Biodegradable Metals. *Mater. Sci. Eng. R Rep.* **2014**, *77*, 1–34. [CrossRef]
2. Tang, Z.; Niu, J.; Huang, H.; Zhang, H.; Pei, J.; Ou, J.; Yuan, G. Potential Biodegradable Zn-Cu Binary Alloys Developed for Cardiovascular Implant Applications. *J. Mech. Behav. Biomed. Mater.* **2017**, *72*, 182–191. [CrossRef] [PubMed]
3. Tan, L.; Yu, X.; Wan, P.; Yang, K. Biodegradable Materials for Bone Repairs: A Review. *J. Mater. Sci. Technol.* **2013**, *29*, 503–513. [CrossRef]
4. Moravej, M.; Mantovani, D. Biodegradable Metals for Cardiovascular Stent Application: Interests and New Opportunities. *Int. J. Mol. Sci.* **2011**, *12*, 4250–4270. [CrossRef]
5. Liu, X.; Sun, J.; Zhou, F.; Yang, Y.; Chang, R.; Qiu, K.; Pu, Z.; Li, L.; Zheng, Y. Micro-Alloying with Mn in Zn–Mg Alloy for Future Biodegradable Metals Application. *Mater. Des.* **2016**, *94*, 95–104. [CrossRef]
6. Levy, G.K.; Goldman, J.; Aghion, E. The Prospects of Zinc as a Structural Material for Biodegradable Implants—A Review Paper. *Metals* **2017**, *7*, 402. [CrossRef]
7. Aghion, E.; Yered, T.; Perez, Y.; Gueta, Y. The Prospects of Carrying and Releasing Drugs via Biodegradable Magnesium Foam. *Adv. Eng. Mater.* **2010**, *12*, B374–B379. [CrossRef]
8. Han, C.; Fang, Q.; Shi, Y.; Tor, S.B.; Chua, C.K.; Zhou, K. Recent Advances on High-Entropy Alloys for 3D Printing. *Adv. Mater.* **2020**, *32*, e1903855. [CrossRef]
9. Wang, D.; Liu, L.; Deng, G.; Deng, C.; Bai, Y.; Yang, Y.; Wu, W.; Chen, J.; Liu, Y.; Wang, Y.; et al. Recent progress on additive manufacturing of multi-material structures with laser powder bed fusion. *Virtual Phys. Prototyp.* **2022**, *17*, 329–365. [CrossRef]
10. Shen, C.; Liu, X.; Fan, B.; Lan, P.; Zhou, F.; Li, X.; Wang, H.; Xiao, X.; Li, L.; Zhao, S.; et al. Mechanical Properties, in Vitro Degradation Behavior, Hemocompatibility and Cytotoxicity Evaluation of Zn–1.2 Mg Alloy for Biodegradable Implants. *RSC Adv.* **2016**, *6*, 86410–86419. [CrossRef]

11. Niinomi, M. Metallic biomaterials. *J. Artif. Organs* **2008**, *11*, 105–110. [CrossRef]
12. Aksakal, B.; Yildirim, S.; Gul, H. Metallurgical failure analysis of various implant materials used in orthopedic applications. *J. Fail. Anal. Prev.* **2004**, *4*, 17–23. [CrossRef]
13. Pospíšilová, I.; Soukupová, V.; Vojtěch, D. Influence of Calcium on the Structure and Mechanical Properties of Biodegradable Zinc Alloys. In *Materials Science Forum*; Trans Tech Publications Ltd.: Freienbach, Switzerland, 2017.
14. Schinhammer, M.; Hänzi, A.C.; Löffler, J.F.; Uggowitzer, P.J. Design Strategy for Biodegradable Fe-Based Alloys for Medical Applications. *Acta Biomater.* **2010**, *6*, 1705–1713. [CrossRef]
15. Liu, B.; Zheng, Y.F. Effects of Alloying Elements (Mn, Co, Al, W, Sn, B, C and S) on Biodegradability and in Vitro Biocompatibility of Pure Iron. *Acta Biomater.* **2011**, *7*, 1407–1420. [CrossRef]
16. Montani, M.; Demir, A.G.; Mostaed, E.; Vedani, M.; Previtali, B. Processability of pure Zn and pure Fe by SLM for biodegradable metallic implant manufacturing. *Rapid Prototyp. J.* **2017**, *23*, 514–523. [CrossRef]
17. Feng, Q.; Zhang, D.; Xin, C.; Liu, X.; Lin, W.; Zhang, W.; Chen, S.; Sun, K. Characterization and in vivo evaluation of a bio-corrodible nitrided iron stent. *J. Mater. Sci. Mater. Med.* **2012**, *24*, 713–724. [CrossRef]
18. Kraus, T.; Moszner, F.; Fischerauer, S.; Fiedler, M.; Martinelli, E.; Eichler, J.; Witte, F.; Willbold, E.; Schinhammer, M.; Meischel, M.; et al. Biodegradable Fe-Based Alloys for Use in Osteosynthesis: Outcome of an in Vivo Study after 52 Weeks. *Acta Biomater.* **2014**, *10*, 3346–3353. [CrossRef]
19. Schinhammer, M.; Gerber, I.; Hänzi, A.C.; Uggowitzer, P.J. On the Cytocompatibility of Biodegradable Fe-Based Alloys. *Mater. Sci. Eng. C* **2013**, *33*, 782–789. [CrossRef]
20. Chen, H.; Zhang, E.; Yang, K. Microstructure, corrosion properties and bio-compatibility of calcium zinc phosphate coating on pure iron for biomedical application. *Mater. Sci. Eng. C* **2013**, *34*, 201–206. [CrossRef]
21. Kafri, A.; Ovadia, S.; Yosafovich-Doitch, G.; Aghion, E. The Effects of 4%Fe on the Performance of Pure Zinc as Biodegradable Implant Material. *Ann. Biomed. Eng.* **2019**, *47*, 1400–1408. [CrossRef]
22. Aghion, E.; Bronfin, B.; Eliezer, D.; Von Buch, F.; Schumann, S.; Friedrich, H.E. The Art of Developing New Magnesium Alloys for High Temperature Applications. In *Materials Science Forum*; Trans Tech Publications Ltd: Freienbach, Switzerland, 2003.
23. Staiger, M.P.; Pietak, A.M.; Huadmai, J.; Dias, G. Magnesium and Its Alloys as Orthopedic Biomaterials: A Review. *Biomaterials* **2006**, *27*, 1728–1734. [CrossRef] [PubMed]
24. Witte, F. The History of Biodegradable Magnesium Implants: A Review. *Acta Biomater.* **2010**, *6*, 1680–1692. [CrossRef] [PubMed]
25. Witte, F.; Fischer, J.; Nellesen, J.; Crostack, H.A.; Kaese, V.; Pisch, A.; Beckmann, F.; Windhagen, H. In Vitro and in Vivo Corrosion Measurements of Magnesium Alloys. *Biomaterials* **2006**, *27*, 1013–1018. [CrossRef] [PubMed]
26. Song, G. Control of Biodegradation of Biocompatable Magnesium Alloys. *Corros. Sci.* **2007**, *49*, 1696–1701. [CrossRef]
27. Kafri, A.; Ovadia, S.; Yosafovich-Doitch, G.; Aghion, E. In vivo performances of pure Zn and Zn–Fe alloy as biodegradable implants. *J. Mater. Sci. Mater. Med.* **2018**, *29*, 94. [CrossRef]
28. Esmaily, M.; Svensson, J.E.; Fajardo, S.; Birbilis, N.; Frankel, G.S.; Virtanen, S.; Arrabal, R.; Thomas, S.; Johansson, L.G. Fundamentals and Advances in Magnesium Alloy Corrosion. *Prog. Mater. Sci.* **2017**, *89*, 92–193. [CrossRef]
29. Aghion, E.; Gueta, Y.; Moscovitch, N.; Bronfin, B. Effect of yttrium additions on the properties of grain-refined Mg–3%Nd alloy. *J. Mater. Sci.* **2008**, *43*, 4870–4875. [CrossRef]
30. Avior, O.; Ben Ghedalia-Peled, N.; Ron, T.; Vago, R.; Aghion, E. The Effect of Ca on In Vitro Behavior of Biodegradable Zn-Fe Alloy in Simulated Physiological Environments. *Metals* **2020**, *10*, 1624. [CrossRef]
31. Hänzi, A.C.; Gerber, I.; Schinhammer, M.; Löffler, J.F.; Uggowitzer, P.J. On the in Vitro and in Vivo Degradation Performance and Biological Response of New Biodegradable Mg–Y–Zn Alloys. *Acta Biomater.* **2010**, *6*, 1824–1833. [CrossRef]
32. Cha, P.R.; Han, H.S.; Yang, G.F.; Kim, Y.C.; Hong, K.H.; Lee, S.C.; Jung, J.Y.; Ahn, J.P.; Kim, Y.Y.; Cho, S.Y.; et al. Biodegradability Engineering of Biodegradable Mg Alloys: Tailoring the Electrochemical Properties and Microstructure of Constituent Phases. *Sci. Rep.* **2013**, *3*, 2367. [CrossRef]
33. Manivasagam, G.; Suwas, S. Biodegradable Mg and Mg based alloys for biomedical implants. *Mater. Sci. Technol.* **2014**, *30*, 515–520. [CrossRef]
34. Maier, P.; Hort, N. Magnesium Alloys for Biomedical Applications. *Metals* **2020**, *10*, 1328. [CrossRef]
35. Jia, B.; Yang, H.; Han, Y.; Zhang, Z.; Qu, X.; Zhuang, Y.; Wu, Q.; Zheng, Y.; Dai, K. In Vitro and in Vivo Studies of Zn-Mn Biodegradable Metals Designed for Orthopedic Applications. *Acta Biomater.* **2020**, *108*, 358–372. [CrossRef]
36. Zhou, C.; Li, H.F.; Yin, Y.X.; Shi, Z.Z.; Li, T.; Feng, X.Y.; Zhang, J.W.; Song, C.X.; Cui, X.S.; Xu, K.L.; et al. Long-Term in Vivo Study of Biodegradable Zn-Cu Stent: A 2-Year Implantation Evaluation in Porcine Coronary Artery. *Acta Biomater.* **2019**, *97*, 657–670. [CrossRef]
37. Jia, B.; Yang, H.; Zhang, Z.; Qu, X.; Jia, X.; Wu, Q.; Han, Y.; Zheng, Y.; Dai, K. Biodegradable Zn–Sr Alloy for Bone Regeneration in Rat Femoral Condyle Defect Model: In Vitro and in Vivo Studies. *Bioact. Mater.* **2021**, *6*, 1588–1604. [CrossRef]
38. Berg, J.M.; Shi, Y. The Galvanization of Biology: A Growing Appreciation for the Roles of Zinc. *Science* **1996**, *271*, 1081–1085. [CrossRef]
39. Shi, Z.-Z.; Li, Z.-L.; Bai, W.-S.; Tuoliken, A.; Yu, J.; Liu, X.-F. (Fe, Mn)Zn_{13} phase and its core-shell structure in novel biodegradable Zn-Mn-Fe alloys. *Mater. Des.* **2019**, *162*, 235–245. [CrossRef]
40. Thian, E.S.; Konishi, T.; Kawanobe, Y.; Lim, P.N.; Choong, C.; Ho, B.; Aizawa, M. Zinc-substituted hydroxyapatite: A biomaterial with enhanced bioactivity and antibacterial properties. *J. Mater. Sci. Mater. Med.* **2012**, *24*, 437–445. [CrossRef]

41. Wei, Z.; Burwinkel, M.; Palissa, C.; Ephraim, E.; Schmidt, M.F. Antiviral Activity of Zinc Salts against Transmissible Gastroenteritis Virus in Vitro. *Vet. Microbiol.* **2012**, *160*, 468–472. [CrossRef]
42. Russell, R.; Beard, J.; Cousins, R.; Dunn, J.T.; Ferland, G.; Hambidge, K.M.; Lynch, S.; Penland, J.; Ross, A.C.; Stoeker, B.J.; et al. A report of the panel. In *Dietary Reference Intakes for Vitamin A, Vitamin K, Arsenic, Boron, Chromium, Copper, Iodine, Iron, Manganese, Molybdenum, Nickel, Silicon, Vanadium, and Zinc*; The National Academies Press: Washington, DC, USA, 2001. [CrossRef]
43. Soetan, K.O.; Olaiya, C.O.; Oyewole, O.E. The Importance of Mineral Elements for Humans, Domestic Animals and Plants—A Review. *Afr. J. Food Sci.* **2010**, *4*, 200–222.
44. Shi, Z.Z.; Yu, J.; Liu, X.F. Microalloyed Zn-Mn Alloys: From Extremely Brittle to Extraordinarily Ductile at Room Temperature. *Mater. Des.* **2018**, *144*, 343–352. [CrossRef]
45. Itzhak, D.; Aghion, E. An Anodic Behaviour Study of an Analogical Sintered System of Austenitic Stainless Steel in H_2SO_4 Solution. *Corros. Sci.* **1984**, *24*, 145–149. [CrossRef]
46. Wang, J.; Witte, F.; Xi, T.; Zheng, Y.; Yang, K.; Yang, Y.; Zhao, D.; Meng, J.; Li, Y.; Li, W.; et al. Recommendation for Modifying Current Cytotoxicity Testing Standards for Biodegradable Magnesium-Based Materials. *Acta Biomater.* **2015**, *21*, 237–249. [CrossRef] [PubMed]
47. Li, P.; Schille, C.; Schweizer, E.; Rupp, F.; Heiss, A.; Legner, C.; Klotz, U.E.; Geis-Gerstorfer, J.; Scheideler, L. Mechanical Characteristics, in Vitro Degradation, Cytotoxicity, and Antibacterial Evaluation of Zn-4.0 Ag Alloy as a Biodegradable Material. *Int. J. Mol. Sci.* **2018**, *19*, 755. [CrossRef]
48. Bhan, S.; Lal, A.; Singh, S. The Fe-Mn-Zn system (iron-manganese-zinc). *J. Phase Equilibria Diffus.* **1991**, *12*, 667–672. [CrossRef]
49. Lee, H.H.; Hiam, D. Corrosion Resistance of Galvannealed Steel. *Corrosion* **1989**, *45*, 852–856. [CrossRef]
50. *ISO 10993-12*; Biological Evaluation of Medical Devices—Part 12: Sample Preparation and Reference Materials. International Organization for Standardization (ISO): Geneva, Switzerland, 2012.
51. Chen, Y.; Xu, Z.; Smith, C.; Sankar, J. Recent Advances on the Development of Magnesium Alloys for Biodegradable Implants. *Acta Biomater.* **2014**, *10*, 4561–4573. [CrossRef]
52. Avedesian, M.; Baker, H. *ASM Specialty Handbook: Magnesium and Magnesium Alloys*; ASM International: Washington, DC, USA, 1999.
53. Bronfin, B.; Aghion, E.; von Buch, F.; Schumann, S.; Katsir, M. Die Casting Magnesium Alloys for Elevated Temperatures Applications. In Proceedings of the Magnesium Technology 2001, New Orleans, LA, USA, 11–15 February 2001. [CrossRef]
54. Vanýsek, P. Electrochemical Series. In *Handbook of Chemistry and Physics*, 93rd ed.; Haynes, W.M., Ed.; CRC Press: Boca Raton, FL, USA, 2012; pp. 5–80.
55. Prasadh, S.; Gupta, M.; Wong, R. In Vitro Cytotoxicity and Osteogenic Potential of Quaternary Mg-2Zn-1Ca/X-Mn Alloys for Craniofacial Reconstruction. *Sci. Rep.* **2022**, *12*, 8259. [CrossRef]
56. Wang, J.; Huang, S.; Li, Y.; Wei, Y.; Xi, X.; Cai, K. Microstructure, Mechanical and Bio-Corrosion Properties of Mn-Doped Mg–Zn–Ca Bulk Metallic Glass Composites. *Mater. Sci. Eng. C* **2013**, *33*, 3832–3838. [CrossRef]
57. Wang, J.-L.; Wan, Y.; Ma, Z.-J.; Guo, Y.-C.; Yang, Z.; Wang, P.; Li, J.-P. Glass-forming ability and corrosion performance of Mn-doped Mg–Zn–Ca amorphous alloys for biomedical applications. *Rare Met.* **2018**, *37*, 579–586. [CrossRef]